

Bis(imino)pyrazine-Supported Iron Complexes: Ligand-Based Redox Chemistry, Dearomatization, and Reversible C–C Bond Formation

Nicolas I. Regenauer, Simon Settele, Eckhard Bill, Hubert Wadepohl, and Dragoş-Adrian Roşca*

Cite This: <https://dx.doi.org/10.1021/acs.inorgchem.9b03665>

Read Online

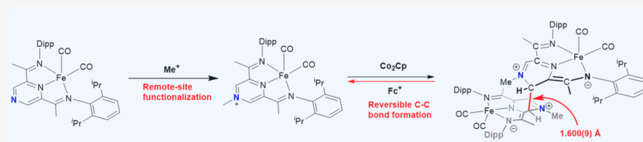
ACCESS |

Metrics & More

Article Recommendations

Supporting Information

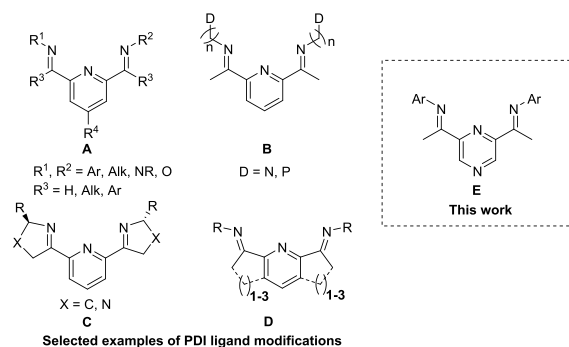
ABSTRACT: Iron complexes supported by novel π -acidic bis(imino)pyrazine (P^{PzDI}) ligands can be functionalized at the nonligated nitrogen atom, and this has a marked effect on the redox properties of the resulting complexes. Dearomatization is observed in the presence of cobaltocene, which reversibly reduces the pyrazine core and not the imine functionality, as observed in the case of the pyridinediimine-ligated iron analogues. The resulting ligand-based radical is prone to dimerization through the formation of a long carbon–carbon bond, which can be subsequently cleaved under mild oxidative conditions.



INTRODUCTION

Pyridinediimine ligands (PDI) represent a privileged class of scaffolds, capable of stabilizing a wide range of transition metals in a variety of oxidation states. Brookhart and Gibson demonstrated their unique role in the chemistry of iron and cobalt, where the corresponding complexes can act as catalysts for ethylene polymerization.¹ Since these original reports published two decades ago, the interest in first-row-transition-metal-based PDI ligands has substantially increased, prompted by wide catalytic applications in a series of challenging transformations, such as cycloadditions,² hydroelementation reactions of unsaturated C–C³ and C–O bonds,⁴ and coupling of CO₂ with ethylene.⁵ The reported reactivity competes with and occasionally even surpasses that reported for noble-metal catalysts.⁶ The key to success is closely related to the electronic structure of the catalysts, which facilitates two-electron-redox processes, even for metals where one-electron transfer is the most accessible thermodynamic and kinetic pathway. PDI ligands achieve this by acting as an electron reservoir for the metal center, thereby being able to reversibly accept electrons, depending on the specific requirements of the transformation.⁷ This feature enables these systems to stabilize key species, such as dinitrogen, carbene, or imido fragments,⁸ and therefore have been investigated spectroscopically and computationally in detail by Chirik, Wieghardt, and others.^{9,10} As it has been recognized that subtle electronic and steric changes can have an important effect on reactivity and electronic structure, synthetic work has also focused on modifying the initial ligand scaffold, which has given rise to powerful new catalytic systems for the targeted applications. For example, it has been shown that increasing the steric bulk of R³ (A, Chart 1) can change the ground state in iron dinitrogen complexes stabilized by PDI ligands.^{10c} Replacing the aromatic group on the imine nitrogen atom with cyclohexyl switches the selectivity in the hydroboration of terminal alkynes,¹¹ while introducing a pendant phosphine arm or amine on this position yields

Chart 1. Various Developments of Catalytically Relevant PDI-Type Ligands



efficient catalysts for ketone hydrosilylation and NO₂[−] reduction (B, Chart 1).¹² Chiral information could be introduced in the PDI backbone by employing chiral oxazolines, which gives rise to the well-established PyBox ligand family (C, Chart 1).¹³ Furthermore, the imine fragment could be tethered to the meta position of the heterocyclic core in order to control the metal–imine dissociation rates (D, Chart 1), with important consequences in cycloaddition reactions and selective oligomerization of ethylene (Figure 1).¹⁴

As the catalytic properties and the electronic structure of PDI-based metal complexes seem to be very sensitive to the electronic density around the metal center,¹⁵ we have envisaged that enhancing the π acidity of the N-heterocycle

Received: December 17, 2019

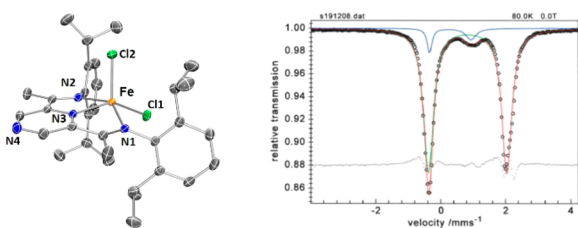


Figure 1. Solid-state characterization data for **8**. (left) Molecular structure obtained by single-crystal X-ray diffraction. Hydrogen atoms are omitted for clarity. (right) Zero-field ^{57}Fe Mössbauer spectrum recorded at 80 K. The red line represents a fit with a Lorentzian quadrupole doublet with the following parameters: $\delta = 0.83 \text{ mm s}^{-1}$, $|\Delta E_Q| = 2.42 \text{ mm s}^{-1}$. The deviations indicate a 8% contamination with an unknown species with the following fitted parameters: $\delta = 0.30 \text{ mm s}^{-1}$, $|\Delta E_Q| = 1.28 \text{ mm s}^{-1}$.

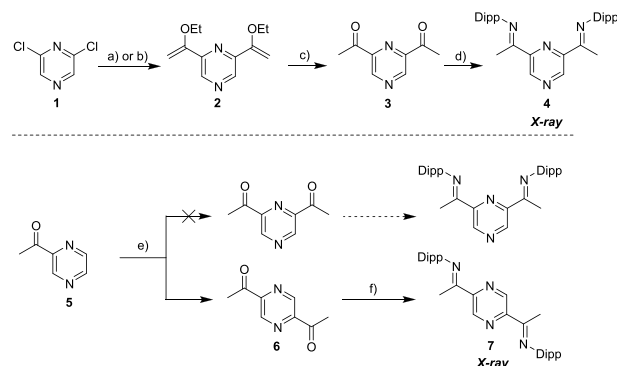
would facilitate the delocalization of electrons from the metal onto the ligand. For this task, we have sought to replace the pyridine core with pyrazine, which would bring the following assets: (i) pyrazine is a strong π acceptor with the lowest $\pi-\pi^*$ transitions documented to be about 0.95 eV smaller those of than pyridine,¹⁶ while its basicity is reduced by about 5 orders of magnitude ($\text{p}K_a$ 1.30 vs 5.20 in pyridine),¹⁷ (ii) the N atom can stabilize transient species in various transformations via intermolecular coordination, and (iii) the nitrogen atom in the 4-position can be further functionalized through alkylation, protonation, or reactions with Lewis acids, which have an important influence on the electron density around the metal center. This functionality has been recently explored by Tilley, Bergman, and others in bipyrazine- or bipyrimidine-based palladium and platinum systems, where they have shown that a coordination of a Lewis acid can alter the redox potential by 600 mV and enhance the rate of reductive elimination by up to 10^8 in comparison to control experiments.¹⁸

RESULTS AND DISCUSSION

The synthesis of the ligand class type E (Chart 1) was achieved via a three-step synthesis, starting from 2,6-dichloropyrazine (**1**). A Stille coupling under low catalytic loading (2.5 mol %) furnished the divinyl ether **2**, which was hydrolyzed under mild acidic conditions to the analogous diketone **3**. Finally, an acid-catalyzed condensation with 2,6-diisopropylaniline afforded the target pyrazinediimine ligand (P^{PzDI}). The reaction sequence could be conducted on scale, furnishing 7 g of **4** in an overall yield of 47%. A Ni-catalyzed Negishi coupling could also be used to obtain the divinyl ether **2**; however, this method requires a relatively high catalytic loading and large excess of the zinc nucleophile. Moreover, attempting to use this method on scale (>3 g) results in a considerable drop in isolated yield.

The mild palladium-catalyzed route is orthogonal to the other general synthetic pathways employed for the synthesis of PDI-type ligands.¹⁹ The desired connectivity could also be confirmed by single-crystal X-ray diffraction (see the Supporting Information). We note, however, that a previously reported synthesis for **4**,²⁰ which would be achieved via a Minisci coupling between an acyl radical generated from pyruvic acid and 2-acylpyrazine **5** followed by an acid-catalyzed condensation with 2,6-diisopropylaniline, yielded the (wrong) 2,5-isomer **7** (Scheme 1), as established through our single-crystal X-ray diffraction studies (see the Supporting Information).²¹

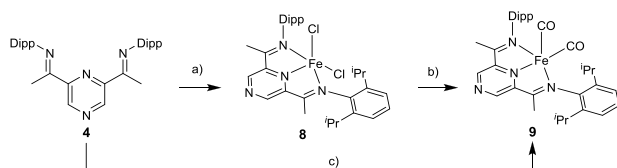
Scheme 1^a



^aReagents and conditions: (a) tributyl(1-ethoxyvinyl)stannane (2.3 equiv), $\text{Pd}(\text{PPh}_3)_2\text{Cl}_2$ (2.5 mol %), toluene, 120 °C, 76%; (b) (1-ethoxyvinyl)zinc chloride (6 equiv), $\text{Ni}(\text{dppp})\text{Cl}_2$ (10 mol %), THF/dioxane, 70 °C, 40%; (c) HCl (1 M aqueous), THF, 80%; (d) DippNH_2 , $\text{PTSA}\cdot\text{H}_2\text{O}$ (15 mol %), toluene, 140 °C, 77% ($\text{Dipp} = 2,6$ -diisopropylphenyl, $\text{PTSA} = p$ -toluenesulfonic acid); (e) H_2SO_4 (98% aqueous), pyruvic acid, $(\text{NH}_4)_2\text{S}_2\text{O}_8$, AgNO_3 , H_2O , 50 °C, 25%; (f) DippNH_2 , MeOH, HOAc, reflux, 75%.

In order to evaluate the redox properties of **4** against a well-established backdrop, we decided to initially turn our attention to the iron chemistry of this system. Treating a THF solution of FeCl_2 with **4** at room temperature affords $(\text{P}^{\text{PzDI}}\text{DI})\text{FeCl}_2$ (**8**) as a green paramagnetic solid in very good yield. The solution magnetic moment ($\mu_{\text{eff}} = 4.96 \mu_{\text{B}}$, Evans method) is characteristic for a high-spin Fe(II) complex ($S = 2$) (Scheme 2). Despite the paramagnetic character, the ^1H and ^{13}C spectra are well resolved (see the Supporting Information).

Scheme 2^a



^aReagents and conditions: (a) FeCl_2 , THF, 92%; (b) Na/Hg, CO (1 atm), toluene, 40%; (c) $(\text{bda})\text{Fe}(\text{CO})_3$, toluene, 110 °C, 70% ($\text{bda} = \text{benzylideneacetone}$).

Single-crystal X-ray analysis (Figure 1, left) shows that, under the crystallization conditions employed, complex **8** is monomeric and the unligated pyrazine nitrogen atom is not engaged in coordination with a neighboring molecule.²² The geometry around the metal center is best described as a distorted square pyramid ($\tau = 0.36$),²³ with Fe–Cl bond distances essentially identical with those of $(\text{iPr}^{\text{PDI}})\text{FeCl}_2$ (for **8**, Fe–Cl1 2.2561(4) Å and Fe–Cl2 2.3041(4) Å; for $(\text{iPr}^{\text{PDI}})\text{FeCl}_2$,^{1a,b} Fe–Cl1 2.266(2) Å and Fe–Cl2 2.311(2) Å). The other metrical data (vide infra) and Mössbauer spectroscopy (Figure 1, right) further confirm the structure of **8** as a high-spin Fe(II) complex, bound to a neutral P^{PzDI} scaffold.

Subjecting **8** to 1 atm of CO under reducing conditions (Na/Hg) affords $(\text{P}^{\text{PzDI}}\text{DI})\text{Fe}(\text{CO})_2$ (**9**) in moderate yield (40%). The reaction byproduct was invariably proligand **4**, which displays solubility properties similar to those of **9**, ensuring a difficult separation from the reaction mixture. To

circumvent this, we sought to obtain **9** directly by reacting **4** with an Fe(0) source such as (bda)Fe(CO)₃ (bda = benzylideneacetone), relying on the facile displacement of bda under thermolytic conditions. This method allows access to **9** on scale, in good isolated yields (Scheme 2), and avoids the use of large quantities of mercury. The formally Fe(0) complex is obtained as a green, diamagnetic solid, with a C_{2v} symmetry in solution, as observed by NMR spectroscopy. It displays good solubility in all common organic solvents, including pentane, from which the compound could be recrystallized. The molecular structure (Figure 2, left) confirms

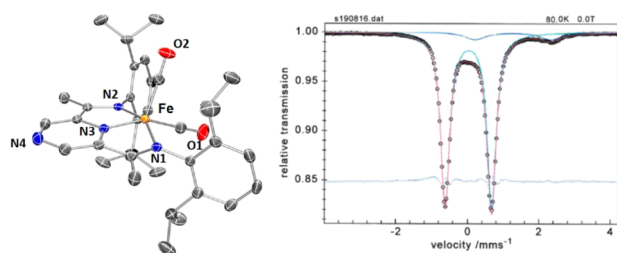


Figure 2. Solid-state characterization data for **9**. (left) Molecular structure obtained by single-crystal X-ray diffraction. Only one of the two molecules present in the asymmetric unit is displayed. The cocrystallized pentane molecule and hydrogen atoms are omitted for clarity. (right) Zero-field ⁵⁷Fe-Mössbauer spectrum recorded at 80 K. The red line represents a fit with a Lorentzian quadrupole doublet with the following parameters: $\delta = 0.03 \text{ mm s}^{-1}$, $|\Delta E_Q| = 1.29 \text{ mm s}^{-1}$. The deviations at ca. 0 and 2 mm s⁻¹ indicate an 11% contamination with an unknown Fe(II) species.

that the geometry around the metal center is idealized square pyramidal ($\angle \text{OC-Fe-CO} = 94.63(9)^\circ$), while the N₂-C_{imine}/C_{imine}-C_{ipso} and C_{ipso}-N₃ bond distances are nearly identical with those of (iPrPDI)Fe(CO)₂ (for **9**, N₂-C_{imine} 1.326(2) Å, C_{imine}-C_{ipso} 1.432(3) Å, and C_{ipso}-N₃ 1.375(2) Å; for (iPrPDI)Fe(CO)₂,^{10b} N₂-C_{imine} 1.332(2) Å, C_{imine}-C_{ipso} 1.428(3) Å, and C_{ipso}-N₃ 1.379(2) Å).

The solid-state IR (ATR, Table 1) spectrum of **9** displays two absorptions in a 0.9:1.1 intensity ratio, suggesting two

Table 1. ¹⁵N NMR Data and Infrared Stretches ν_{CO} for Complexes **4**, **9**, [10]·I, **11**, and (PDI)Fe(CO)₂

complex	¹⁵ N NMR ^a			IR (ν_{CO})	
	δ_{N1}	δ_{N2}	δ_{N4}	solid ^b	soln
4	345.8	<i>c</i>	321.8		
(PDI)Fe(CO) ₂	255.0	<i>c</i>		1946, 1888	1974, 1914 ^e
9	250.8	<i>c</i>	<i>d</i>	1967, 1904	1984, 1925 ^e
[10]·I	261.9	<i>c</i>	145.5	1999, 1938	2010, 1952 ^f
11	222.9	185.9	80.8	1955, 1889	1972, 1907 ^e

^aDetermined by ¹H-¹⁵N HMBC. ^bIR-ATR. ^c $\delta_{\text{N1}} = \delta_{\text{N2}}$. ^dNot observable. ^eIn pentane. ^fIn CH₂Cl₂.

nonequivalent CO ligands, as confirmed by single-crystal X-ray diffraction. The ν_{CO} stretching frequencies of **9** (1967, 1904 cm⁻¹) are slightly shifted to higher frequencies in comparison to those in (iPrPDI)Fe(CO)₂ (1946, 1888 cm⁻¹),²⁴ suggesting a greater π acidity of pyrazine in comparison to pyridine, therefore reducing back-bonding to the carbonyl ligands. The increased π acidity of the pyrazine is also reflected in the redox potentials of **4** and **9**. Proligand **4** displays a reversible reduction wave in THF solution at a peak potential of -2.36 V

(vs ferrocene), shifted anodically by 260 mV in comparison to the iPrPDI ligand (-2.62 V vs ferrocene) and very similar to that of the 4-CF₃-iPrPDI ligand (-2.35 V vs ferrocene) (Figure 3).^{19b} Complex **9** displays one reversible oxidation event at a

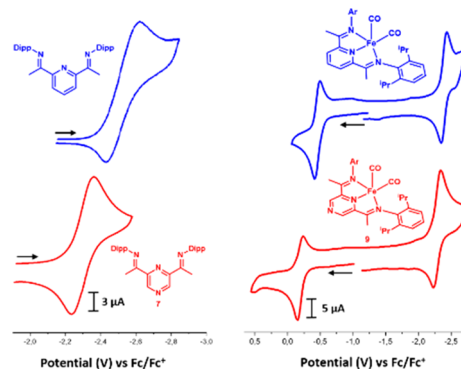


Figure 3. Cyclic voltammetry (glassy-carbon working electrode, 0.1 M (nBu₄N)[B(C₆F₅)₄], scan rate 100 mV s⁻¹ in THF at 295 K versus ferrocene^{0/+}): (left) overlay of iPrPDI (blue) and iPrPzDI (red) (**4**); (right) overlay of iPr(PDI)Fe(CO)₂ (blue) and iPr(PzDI)Fe(CO)₂ (red) (**9**).

peak potential of -0.23 V (vs ferrocene) and one reversible reduction event at -2.28 V (vs ferrocene), both anodically shifted by 260 and 180 mV, respectively, in comparison to (iPrPDI)Fe(CO)₂ (-0.49 and -2.46 V vs ferrocene). In analogy to the studies reported by Chirik, we assign the oxidation wave to be metal-based (Fe⁰ to Fe^I) and the reduction wave to be ligand-based (L to L⁻).²⁵ The data suggest that the magnitude of the HOMO-LUMO gaps are similar, where the levels of the frontier orbitals in (P^{Pz}DI)Fe(CO)₂ would be lower in comparison to the (PDI)Fe(CO)₂ analogue, which was also confirmed by computing the energetic levels of the frontier orbitals (vide infra). The oxidation state of the formally Fe(0) carbonyl complexes supported by potentially noninnocent iminopyridine-based PNN and PDI systems has been previously discussed in great depth and assessed through combined spectroscopic and computational means.²⁶ Metrical parameters obtained from single-crystal diffractometry, especially the N₂-C_{imine}/C_{imine}-C_{ipso} and C_{ipso}-N₃ bond distances, have been found to have diagnostic value in distinguishing between Fe⁰ species bound by a neutral ligand, LFe⁰(CO)₂, and an Fe^{II} species antiferromagnetically coupled to a reduced ligand diradical, L^{•2-}Fe^{II}(CO)₂. In the case of **9**, the N₂-C_{imine} and C_{ipso}-N₃ bond distances appear significantly elongated while the C_{imine}-C_{ipso} bond is significantly contracted in comparison to those in the free ligand **4** and (P^{Pz}DI)FeCl₂ (**8**) (Figure 4). The bond distances are similar to those computed for the monoanionic form of the α -iminopyridine of 1.34, 1.41, and 1.39 Å respectively,⁹ while Wieghardt's single structural parameter $\Delta_{\text{exp}} = 0.0772$ ($\Delta_{\text{calc}}(\text{DFT}, \text{B3LYP}) = 0.0767$; vide infra) suggests an important contribution from the resonance structure consisting of direduced (P^{Pz}DI)^{•2-}.²⁷ In line with this interpretation, ¹⁵N NMR of the imine nitrogen atom (N=C) also shows a significant upfield shift in complex **9** ($\delta_{\text{N}} 250.8$), in comparison to that in the free ligand **4** ($\delta_{\text{N}} 345.8$), suggesting an accumulation of charge density on this site. Nevertheless, this phenomenon could be also ascribed to strong back-bonding from an electron-rich Fe(0) center to the P^{Pz}DI ligand, and not necessarily to ligand reduction.

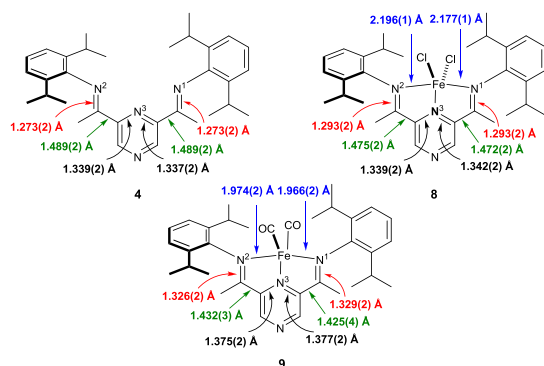


Figure 4. Bond distance comparison among **4**, **8**, and **9**. Mean values are given for the two independent molecules of **4** and **9**. Standard uncertainties are those of individual values. Metric data were obtained from single-crystal X-ray diffraction.

Mössbauer spectroscopy (Figure 2, right) also favors an important contribution from the $\text{LFe}^0(\text{CO})_2$ resonance form, suggesting a zero oxidation state on the iron center ($\delta = 0.03 \text{ mm s}^{-1}$, $|\Delta E_{\text{Q}}| = 1.29 \text{ mm s}^{-1}$).

In order to investigate the potential ligand redox non-innocence, we examined the electronic structures of **8** and **9** by DFT calculations. The structure of compound **8** was modeled through spin-unrestricted DFT calculations at the B3LYP/TZVP(-f) level of theory.²⁸ Geometry optimizations produced structural features which are in good agreement with the metric data obtained from X-ray crystallography. Mössbauer parameters could also be reproduced ($\delta_{\text{calcd}} = 0.75 \text{ mm s}^{-1}$, $\Delta E_{\text{Q(calcd)}} = 2.23 \text{ mm s}^{-1}$),²⁹ supporting the description of compound **8** as a hs-Fe(II) complex. The electronic structure of **9** was analyzed through spin-unrestricted broken-symmetry (BS)³⁰ calculations at the B3LYP/TZVP(-f) level of theory, where three possible formulations were taken into account: (i) $[(\text{P}^{\text{zDI}})^2\text{Fe}^{\text{II}}]$, where a BS(2,2) (quintet) approach was used, (ii) $[(\text{P}^{\text{zDI}})^-\text{Fe}^{\text{I}}]$, where a BS(1,1) (triplet) approach was used, and (iii) $[(\text{P}^{\text{zDI}})\text{Fe}^0]$, where **9** was modeled as an unrestricted singlet. All strategies converged to the same BS(0,0) (i.e. closed-shell) solution, similar to case for the (PDI)Fe(CO)₂ analogue reported by Chirik.²⁵ Additionally, the overlap integrals ($S^{\alpha\beta}$) of the unrestricted corresponding orbitals (UCOs) with values close to unity (for the highest occupied orbitals) provided further evidence for a BS(0,0) ground state.³¹ Therefore, the system was further computed as a closed-shell singlet. The metric parameters of the closed-shell solution are in good agreement with those measured by single-crystal X-ray diffraction, and the calculated Mössbauer parameters ($\delta_{\text{calcd}} = -0.03 \text{ mm s}^{-1}$, $\Delta E_{\text{Q(calcd)}} = 1.28 \text{ mm s}^{-1}$) reproduce well those determined experimentally. On the basis of the experimental and computational data, we therefore favor the $\text{LFe}^0(\text{CO})_2$ formulation. A qualitative molecular orbital diagram comparison between **9** and the pyridine-based analogue (Figure 5) confirms the enhanced π -acceptor character of the pyrazine-based ligand, which is also corroborated by the cyclic voltammetry data (vide supra, Figure 3).

As complex **9** possesses a nitrogen atom amenable for further functionalization, we sought to study the effect of methylation on the electronic properties and reactivity of $(\text{P}^{\text{zDI}})\text{Fe}(\text{CO})_2$ complexes. Reacting complex **9** with a mild methylation reagent such as iodomethane affords the *N*-methylated complex **[10]·I**, isolated as a dark brown

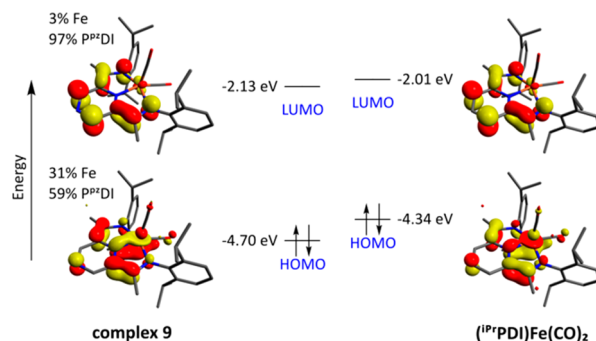
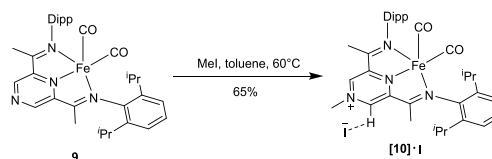


Figure 5. Qualitative molecular orbital diagram comparing the energy levels of complex **9** and the pyridine-based analogue $(\text{iPrPDI})\text{Fe}(\text{CO})_2$ (closed shell singlet, B3LYP, def2-TZVP(-f)). Canonical molecular orbitals are displayed.

diamagnetic powder, insoluble in aliphatic hydrocarbons but partially soluble in aromatic hydrocarbons (Scheme 3). Solid-

Scheme 3



state IR data display two absorptions in a 1:1 intensity, suggesting that the geometry at the metal center would be square pyramidal and thus not influenced by the additional positive charge. The ν_{CO} stretching frequencies are shifted, however, by ca. 30 cm^{-1} to higher frequencies (1999 and 1938 cm^{-1} , Table 1), consistent with the reduced electron density on the iron center, which reduces the back-bonding to the CO ligands.³² For comparison, in a related recent example of the pyridine-based $(\text{PCP})\text{Ru}(\text{CO})_2\text{Cl}$, methylation of the nitrogen atom exerts a more attenuated influence on the ν_{CO} value, from 2023 and 1945 cm^{-1} in $\text{iPr}(\text{PCP})\text{Ru}(\text{CO})_2\text{Cl}$ to 2034 and 1969 cm^{-1} in $[\text{Me}^{\text{iPr}}(\text{PCP})\text{Ru}(\text{CO})_2\text{Cl}]\text{OTf}$. In this case, back-bonding from the metal to the methylated PCP ligand was calculated to be negligible, while in the case of **[10]·I** it would be significant.

¹⁵N NMR spectroscopy (Table 1) reveals that the δ_{N} value of the $\text{C}=\text{N}_{\text{imine}}$ group is slightly shifted downfield (for **9**, δ_{N} 250.8; for **[10]·I**, δ_{N} 261.9), suggesting a decrease in electron density on this site. This interpretation is corroborated by the structural metric data (Figure 6, left) which reveal that, in the

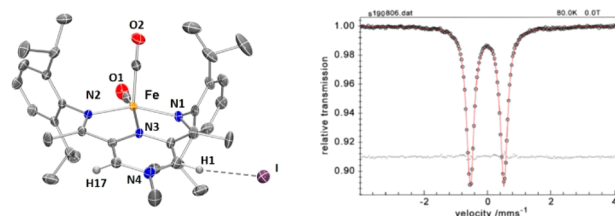


Figure 6. Solid-state characterization data for **[10]·I**. (left) Molecular structure obtained by single-crystal X-ray diffraction. Most hydrogen atoms are omitted for clarity. (right) Zero-field ⁵⁷Fe Mössbauer spectrum recorded at 80 K. The red line represents a fit with a Lorentzian quadrupole doublet with the following parameters: $\delta = 0.00 \text{ mm s}^{-1}$, $|\Delta E_{\text{Q}}| = 1.06 \text{ mm s}^{-1}$.

case of $[10]\cdot\text{I}$, the $\text{N}_2\text{-C}_{\text{imine}}$ bond is slightly contracted in comparison to its nonmethylated congener **9** (1.320(2) Å in $[10]\cdot\text{I}$, 1.326(2) Å in **9**). The Fe-N_3 bonds are also shorter (decreases to 1.810(2) Å in $[10]\cdot\text{I}$ from 1.828(1) Å in **9**),³³ consistent with the ionic character of $[10]\cdot\text{I}$, as well as important back-bonding from Fe to the strongly π accepting pyrazinium core in comparison to **9**. The greater stabilization of pyrazinium cations through back-bonding from a metal center could constitute the driving force in the facile methylation reaction of **9** in the presence of iodomethane. In the absence of the metal, mixing **4** with excess iodomethane (10–20 equiv) for 3 days at 80 °C showed no signs of methylation. The diamagnetic character of $[10]\cdot\text{I}$ is also in line with the Mössbauer data (Figure 6, right) characteristic for a Fe(0) species ($\delta = 0.00 \text{ mm s}^{-1}$, $|\Delta E_{\text{Q}}| = 1.06 \text{ mm s}^{-1}$). N-methylation therefore does not seem to alter the singlet ground state observed in **9**. This could also be corroborated through BS-DFT calculations performed on $[10]\cdot\text{I}$, which converged to a BS(0,0) solution (i.e., closed shell). The calculated Mössbauer parameters based on this solution are also in excellent agreement with the experimentally determined values ($\delta_{\text{calcd}} = -0.02 \text{ mm s}^{-1}$, $\Delta E_{\text{Q(calcd)}} = 1.07 \text{ mm s}^{-1}$). A qualitative molecular orbital diagram comparison between **9** and $[10]\cdot\text{I}$ (Figure 7) reveals that N-methylation reduces significantly the

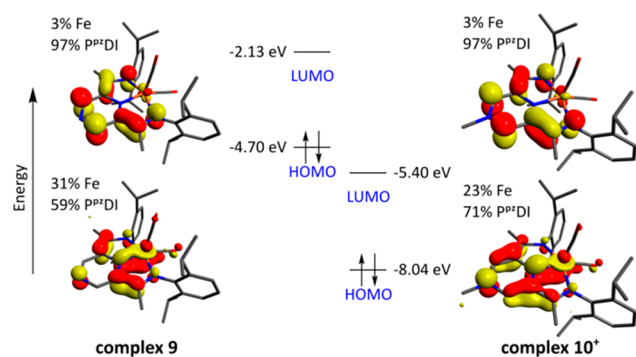


Figure 7. Qualitative molecular orbital diagram illustrating the effect of N-methylation on the energy levels of the frontier orbitals in 10^+ , in comparison to **9** (closed-shell singlet, B3LYP, def2-TZVP(-f)). Canonical molecular orbitals are displayed.

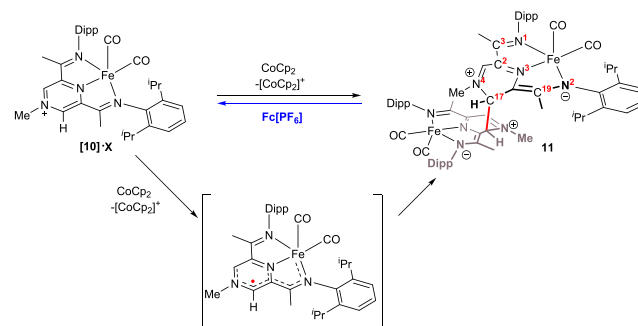
energy of the frontier orbitals in the cationic complex (by 3.27 eV for the LUMO and 3.34 eV for the HOMO), further suggesting an important alteration of the electronic properties of $[10]\cdot\text{I}$.

REDOX CHEMISTRY

Pyridine-based PDI systems coordinated to iron are known to show versatile redox chemistry, where either the metal center or the imine arm can be reduced. Although it is theoretically possible that the heterocyclic core could also be reduced, therefore allowing the PDI system to formally store three electrons, to the best of our knowledge, this has not yet been achieved experimentally. As N-methylated pyrazine systems are considerably more electron poor in comparison to their pyridine congeners, we were wondering if this would enable the reduction of the nitrogen heterocycle in favor of the imine arms. In order to study this, we initially conducted cyclic voltammetry experiments on compound $[10]\cdot\text{I}$, which shows one quasi-reversible wave at a peak potential of -1.53 V (oxidation -1.43 V) and one irreversible wave at -2.10 V (see

the Supporting Information for details). While we can tentatively assign the latter reduction wave to the ligand-based imine reduction (see the CV of **9** above for comparison), we wondered whether the first wave at -1.53 V would correspond to a ligand core reduction. Adding cobaltocene to a benzene suspension of $[10]\cdot\text{I}$ afforded an instant color change from black to purple (Scheme 4). NMR

Scheme 4^a



^aReduction conditions: Cp_2Co (1 equiv), benzene, room temperature, 80% (isolated yield), $\text{X} = \text{I}$; Oxidation conditions: $\text{Fc}[\text{PF}_6]$ (1.4 equiv), C_6D_6 , room temperature, quantitative (NMR yield), $\text{X} = \text{PF}_6$ (substoichiometric amounts of $\text{Fc}[\text{PF}_6]$ were used in order to avoid oxidation of the metal center). The numbering scheme is given for **11**.

analysis reveals the formation of a diamagnetic compound which exhibits a C_1 symmetry in solution. The imine character of the C–N bond on the side of the radical formation is lost, as exhibited by δ_{N_2} 185.9 (compared to δ_{N_1} 222.9) and $\delta_{\text{C}_{19}}$ 141.2 (compared to δ_{C_3} 162.8), while the dearomatization of the pyrazine ring is evident in the pronounced upfield shift of δ_{N_4} 80.8 (compared to δ_{N_4} 145.5 in $[10]\cdot\text{I}$). Single crystal X-ray diffraction (Figure 8, left) shows the formation of a dimeric

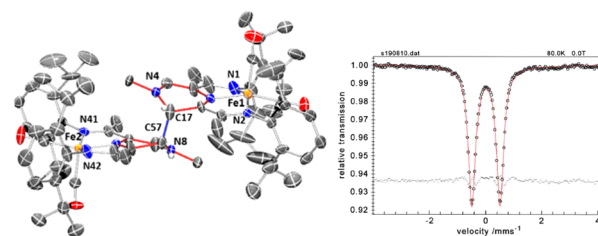


Figure 8. Solid-state characterization data for **11**. (left) Molecular structure obtained by single-crystal X-ray diffraction. Most hydrogen atoms are omitted for clarity. (right) Zero-field ^{57}Fe Mössbauer spectrum recorded at 80 K. The red line represents a fit with a Lorentzian quadrupole doublet with the following parameters: $\delta = 0.02 \text{ mm s}^{-1}$, $|\Delta E_{\text{Q}}| = 0.99 \text{ mm s}^{-1}$.

species, likely obtained through the generation of a radical at the carbon atom α to the cationic nitrogen atom, which subsequently dimerizes to give **11**.³⁴ The dearomatized pyrazine ring deviates significantly from planarity, adopting a distorted-boat conformation. The imine character on the side of the radical formation is attenuated, illustrated through the elongation of the $\text{N}_2\text{-C}_{19}$ bond (1.358(9) Å, in comparison to $\text{N}_1\text{-C}_3$ 1.313(8) Å). Interestingly, the bond created through the radical dimerization appears to be unusually long for a C–C σ bond ($\text{C}_{17}\text{-C}_{57}$ 1.600(9) Å),^{35,36} possibly due to the partial stabilization of the radical character of C_{17} and C_{57} due to the conjugation with the π system, as well as spin

delocalization onto the metal. Nevertheless, Mössbauer spectroscopy suggests a singlet Fe(0) structure, in line with the diamagnetic character observed by NMR spectroscopy (Figure 8, right).

While at least two resonance structures can be envisioned for **11**, taking the spectroscopic and metrical data into account, we suggest the resonance form **B** (Figure 9) to be the dominant one.

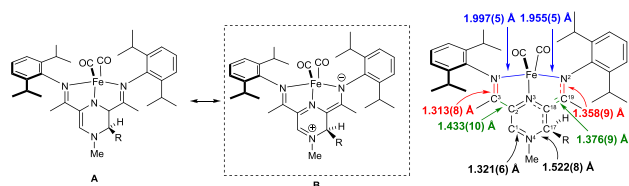


Figure 9. Possible resonance structures and metric data for one dimeric unit of **11** (R = second dimeric unit of **11**).

The long C–C bond formed as a result of radical dimerization prompted us to investigate whether it can be homolytically cleaved under mild oxidizing conditions. Treating a dichloromethane- d_2 solution of **11** with a substoichiometric amount of $\text{Fc}[\text{PF}_6]$ instantly affords $[\mathbf{10}]^+\text{PF}_6^-$ alongside ferrocene, as judged by NMR spectroscopy, showcasing the weak character of the C–C bond as well as the thermodynamic driving force for the rearomatization of the pyrazine ring. Compound **11** represents a rare example of a structurally characterized metal complex where a C–C bond can be cleaved under relatively mild oxidative conditions.³⁷

CONCLUSIONS

In conclusion, we have developed new types of redox-active ligands, where the pyrazine core allows for further functionalization of the unligated nitrogen atom. N-methylation of $(\text{P}^{\text{PzDI}}\text{Fe}(\text{CO})_2)$ proceeds under mild conditions, for which the driving force is the back-bonding stabilization of the resulting cationic species, which is evident in the pronounced effect on the CO stretching frequencies. In contrast to the well-documented pyridine-based PDI chemistry where the imine functionality is most prone to reduction, in the case of N-methylated P^{PzDI} complexes, the pyrazinium core is more easily reduced in comparison to the imine functionality, through the generation of a ligand-based radical. This radical readily dimerizes through the formation of a weak C–C bond which can be subsequently cleaved under mild oxidative conditions. The weak character of the C–C bond suggests that, providing there is enough steric bulk to prevent dimerization, the parent pyrazine-based radical species would be isolable, an endeavor which we are pursuing at the moment.

ASSOCIATED CONTENT

Supporting Information

The Supporting Information is available free of charge at <https://pubs.acs.org/doi/10.1021/acs.inorgchem.9b03665>.

Cartesian coordinates for the calculated structures (XYZ)

Synthesis protocols, spectroscopic data, X-ray crystallographic data, and computational details (PDF)

Accession Codes

CCDC 1968498–1968502 and 1968504 contain the supplementary crystallographic data for this paper. These data can be

obtained free of charge via www.ccdc.cam.ac.uk/data_request/cif, or by emailing data_request@ccdc.cam.ac.uk, or by contacting The Cambridge Crystallographic Data Centre, 12 Union Road, Cambridge CB2 1EZ, UK; fax: +44 1223 336033.

AUTHOR INFORMATION

Corresponding Author

Dragoş-Adrian Roşca – Anorganisch-Chemisches Institut, Universität Heidelberg, 69120 Heidelberg, Germany;

orcid.org/0000-0002-0273-5495; Phone: +49 6221 54 8596; Email: dragos.rosca@uni-heidelberg.de

Authors

Nicolas I. Regenauer – Anorganisch-Chemisches Institut, Universität Heidelberg, 69120 Heidelberg, Germany

Simon Settele – Anorganisch-Chemisches Institut, Universität Heidelberg, 69120 Heidelberg, Germany

Eckhard Bill – Max-Planck-Institut für Chemische Energiekonversion, 45470 Mülheim/Ruhr, Germany;

orcid.org/0000-0001-9138-3964

Hubert Wadepohl – Anorganisch-Chemisches Institut, Universität Heidelberg, 69120 Heidelberg, Germany

Complete contact information is available at:

<https://pubs.acs.org/10.1021/acs.inorgchem.9b03665>

Author Contributions

The manuscript was written through contributions of all authors. All authors have given approval to the final version of the manuscript.

Notes

The authors declare no competing financial interest.

ACKNOWLEDGMENTS

Generous financial support from the Fonds der Chemischen Industrie (FCI) through Liebig research fellowships (N.I.R. and D.-A.R.) is gratefully acknowledged. The computational work was supported by the bwHPC initiative and the bwHPC-C5 project provided through the associated computing services of the JUSTUS HPC facility located at the University of Ulm (Grant INST 40/467-1). We thank Dr. Sorin-Claudiu Roşca (Max-Planck-Institut für Kohlenforschung) and Mr. Bernd Mienert (Max-Planck-Institut für Chemische Energiekonversion) for assistance with the Mössbauer sample preparations and measurements. Priv.-Doz. Joachim Ballmann and Dr. Felix Anderl are acknowledged for helpful discussions, and Prof Lutz H. Gade is acknowledged for continued interest in our work.

REFERENCES

- (1) Original reports: (a) Small, B. L.; Brookhart, M.; Bennett, A. M. Highly Active Iron and Cobalt Catalysts for the Polymerization of Ethylene. *J. Am. Chem. Soc.* **1998**, *120*, 4049–4050. (b) Britovsek, G. J. P.; Gibson, V. C.; Kimberley, B. S.; Maddox, P. J.; Tavish, S. J.; Sloan, G. A.; White, A. J. P.; Williams, D. J. Novel olefin polymerisation catalysts based on iron and cobalt. *Chem. Commun.* **1998**, 849–850. Selected reviews: (c) Bianchini, C.; Giambastani, G.; Rios, I. G.; Mantovani, G.; Meli, A.; Segarra, A. M. Ethylene oligomerization, homopolymerization and copolymerization by iron and cobalt catalysts with 2,6-(bis-organylimino)pyridyl ligands. *Coord. Chem. Rev.* **2006**, *250*, 1391–1418. (d) Gibson, V. C.; Redshaw, C.; Solan, G. A. Bis(imino)pyridines: Surprisingly Reactive Ligands and a Gateway to New Families of Catalysts. *Chem. Rev.* **2007**, *107*, 1745–1776. (e) Flisak, Z.; Sun, W.-H. Progression of Diiminopyridines: From Single Application to Catalytic Versatility. *ACS Catal.* **2015**, *5*, 4713–4724.

- (2) Selected references for Fe. [2 + 2] cycloaddition: (a) Bouwkamp, M. W.; Bowman, A. C.; Lobkovsky, E.; Chirik, P. J. Iron-Catalyzed [2 π +2 π]Cycloaddition of α,ω -Dienes: The Importance of Redox-Active Supporting Ligands. *J. Am. Chem. Soc.* **2006**, *128*, 13340–13341. (b) Hoyt, J. M.; Schmidt, V. A.; Tondreau, A. M.; Chirik, P. J. Iron-catalyzed intermolecular [2 + 2] cycloadditions of unactivated alkenes. *Science* **2015**, *349*, 960–963. (c) Russell, S. K.; Lobkovsky, E.; Chirik, P. J. Iron-Catalyzed Intermolecular [2 π + 2 π] Cycloaddition. *J. Am. Chem. Soc.* **2011**, *133*, 8858–8861. (d) Sylvester, K. T.; Chirik, P. J. Iron-Catalyzed, Hydrogen-Mediated Reductive Cyclization of 1,6-Enynes and Dienes: Evidence of Bis(imino)pyridine Ligand Participation. *J. Am. Chem. Soc.* **2009**, *131*, 8772–8774. [4 + 4] cycloaddition using 2-(imino)pyridine (PI) ligands: (e) Kennedy, C. R.; Zhong, H.; Macaulay, R. L.; Chirik, P. J. Regio- and Diastereoselective Iron-Catalyzed [4 + 4]-Cycloaddition of 1,3-Dienes. *J. Am. Chem. Soc.* **2019**, *141*, 8557–8573.
- (3) (a) Tondreau, A. M.; Atienza, C. C. H.; Weller, K. J.; Nye, S. A.; Lewis, K. M.; Delis, J. G. P.; Chirik, P. J. Iron Catalysis for Selective Anti-Markovnikov Alkene Hydrosilylation Using Tertiary Silanes. *Science* **2012**, *335*, 567–570. (b) Agahi, R.; Challinor, A. J.; Dunne, J.; Docherty, J. H.; Carter, N. B.; Thomas, S. P. Regiodivergent hydrosilylation, hydrogenation, [2 π +2 π]-cycloaddition and C-H borylation using counterion activated earth-abundant metal catalysis. *Chem. Sci.* **2019**, *10*, 5079–5084. (c) Challinor, A. J.; Calin, M.; Nichol, G. S.; Carter, N. B.; Thomas, S. P. Amine-Activated Iron Catalysis: Air- and Moisture-Stable Alkene and Alkyne Hydrofunctionalization. *Adv. Synth. Catal.* **2016**, *358*, 2404–2409. Hydroboration: (d) Agahi, R.; Challinor, A. J.; Carter, N. B.; Thomas, S. P. Earth-Abundant Metal Catalysis Enabled by Counterion Activation. *Org. Lett.* **2019**, *21*, 993–997. (e) Greenhalgh, M.; Thomas, S. P. Chemo-, regio- and stereoselective iron-catalyzed hydrosilylation of alkenes and alkynes. *Chem. Commun.* **2013**, *49*, 11230–11232. Hydromagnesiation: (f) Neate, P. G. N.; Greenhalgh, M. G.; Brennessel, W. W.; Thomas, S. P.; Neidig, S. P. Mechanism of Bis(imino)pyridine-Iron-Catalyzed Hydromagnesiation of Styrene Derivatives. *J. Am. Chem. Soc.* **2019**, *141*, 10099–10108.
- (4) (a) Tondreau, A. M.; Lobkovsky, E.; Chirik, P. J. Bis(imino)pyridine Iron Complexes for Aldehyde and Ketone Hydrosilylation. *Org. Lett.* **2008**, *10*, 2789–2792. For a general review, see: (b) Wei, D.; Darcel, C. Iron Catalysis in Reduction and Hydrometalation Reactions. *Chem. Rev.* **2019**, *119*, 2550–2610. (c) Raya-Baron, C.; Ona-Burgos, P.; Fernandez, I. Iron-Catalyzed Homogeneous Hydrosilylation of Ketones and Aldehydes: Advances and Mechanistic Perspective. *ACS Catal.* **2019**, *9*, 5400–5417.
- (5) Rummelt, S. M.; Zhong, H.; Korobkov, I.; Chirik, P. J. Iron-Mediated Coupling of Carbon Dioxide and Ethylene: Macrocyclic Metallalactones Enable Access to Various Carboxylates. *J. Am. Chem. Soc.* **2018**, *140*, 11589–11593.
- (6) Hojilla Atienza, C. C.; Tondreau, A. M.; Weller, K. J.; Lewis, K. M.; Cruse, R. W.; Nye, S. A.; Boyer, J. L.; Delis, J. G. P.; Chirik, P. J. High-Selectivity Bis(imino)pyridine Iron Catalysts for the Hydrosilylation of 1,2,4-Trivinylcyclohexane. *ACS Catal.* **2012**, *2*, 2169–2172.
- (7) Chirik, P. J.; Wieghardt, K. Radical Ligands Confer Nobility on Base-Metal Catalysts. *Science* **2010**, *327*, 794–795.
- (8) Russell, S. K.; Hoyt, J. M.; Bart, S. C.; Milsmann, C.; Stieber, S. C. E.; Semproni, S. P.; DeBeer, S.; Chirik, P. J. Synthesis, electronic structure and reactivity of bis(imino)pyridine iron carbene complexes: evidence for a carbene radical. *Chem. Sci.* **2014**, *5*, 1168–1174.
- (9) (a) Lu, C. C.; Weyhermüller, T.; Bill, E.; Wieghardt, K. Accessing the Different Redox States of α -Iminopyridines within Cobalt Complexes. *Inorg. Chem.* **2009**, *48*, 6055–6064. (b) Lu, C. C.; Bill, E.; Weyhermüller, T.; Bothe, E.; Wieghardt, K. Neutral Bis(α -iminopyridine)metal Complexes of the First-Row Transition Ions (Cr, Mn, Fe, Co, Ni, Zn) and Their Monocationic Analogues: Mixed Valency Involving a Redox Noninnocent Ligand System. *J. Am. Chem. Soc.* **2008**, *130*, 3181–3197. (c) Lu, C. C.; DeBeer, G. S.; Weyhermüller, T.; Bill, E.; Bothe, E.; Wieghardt, K. An Electron-Transfer Series of High-Valent Chromium Complexes with Redox Non-innocent, Non-Heme Ligands. *Angew. Chem., Int. Ed.* **2008**, *47*, 6384–6387.
- (10) (a) Bart, S. C.; Lobkovsky, E.; Chirik, P. J. Preparation and Molecular and Electronic Structures of Iron(0) Dinitrogen and Silane Complexes and Their Application to Catalytic Hydrogenation and Hydrosilylation. *J. Am. Chem. Soc.* **2004**, *126*, 13794–13807. (b) Bart, S. C.; Chlopek, K.; Bill, E.; Bowkamp, M. W.; Labkovsky, E.; Neese, F.; Wieghardt, K.; Chirik, P. J. Electronic Structure of Bis(imino)pyridine Dichloride, Monochloride, and Neutral Ligand Complexes: A Combined Structural, Spectroscopic, and Computational Study. *J. Am. Chem. Soc.* **2006**, *128*, 13901–13912. (c) Stieber, S. C. E.; Milsmann, C.; Hoyt, J. M.; Turner, Z. R.; Finkelstein, K. D.; Wieghardt, K.; DeBeer, S.; Chirik, P. J. Bis(imino)pyridine Iron Dinitrogen Compounds Revisited: Differences in Electronic Structure between Four- and Five-Coordinate Derivatives. *Inorg. Chem.* **2012**, *51*, 3770–3785.
- (11) Obligacion, J. V.; Neely, J. M.; Yazdani, A. N.; Pappas, I.; Chirik, P. J. Cobalt Catalyzed Z-Selective Hydroboration of Terminal Alkynes and Elucidation of the Origin of Selectivity. *J. Am. Chem. Soc.* **2015**, *137*, 5855–5858.
- (12) (a) Mukhopadhyay, T. K.; Flores, M.; Groy, T. L.; Trovich, R. J. A Highly Active Manganese Precatalyst for the Hydrosilylation of Ketones and Esters. *J. Am. Chem. Soc.* **2014**, *136*, 882–885. (b) Ghosh, C.; Mukhopadhyay, T. K.; Flores, M.; Groy, T. L.; Trovich, R. J. A Pentacoordinate Mn(II) Precatalyst That Exhibits Notable Aldehyde and Ketone Hydrosilylation Turnover Frequencies. *Inorg. Chem.* **2015**, *54*, 10398–10406. (c) Mukhopadhyay, T. K.; Rock, C. L.; Hong, M.; Ashley, D. C.; Groy, T. L.; Baik, M.-H.; Trovich, R. J. Mechanistic Investigation of Bis(imino)pyridine Manganese Catalyzed Carbonyl and Carboxylate Hydrosilylation. *J. Am. Chem. Soc.* **2017**, *139*, 4901–4915. (d) Trovitch, R. J. The Emergence of Manganese-Based Carbonyl Hydrosilylation Catalysts. *Acc. Chem. Res.* **2017**, *50*, 2842–2852. (e) Cheung, P. M.; Burns, K. T.; Kwon, Y. M.; Deshayre, M. Y.; Aguayo, K. J.; Oswald, V. F.; Seda, T.; Zakharov, L. N.; Kowalczyk, T.; Gilbertson, J. D. Hemilabile Proton Relays and Redox Activity Lead to {FeNO}^x and Significant Rate Enhancements in NO₂⁻ Reduction. *J. Am. Chem. Soc.* **2018**, *140*, 17040–17050.
- (13) (a) Desimoni, G.; Faita, G.; Quadrelli, P. Pyridine-2,6-bis(oxazolines), Helpful Ligands for Asymmetric Catalysis. *Chem. Rev.* **2003**, *103*, 3119–3154. (b) Desimoni, G.; Faita, G.; Jørgensen, K. A. C₂-Symmetric Chiral Bis(Oxazoline) Ligands in Asymmetric Catalysis. *Chem. Rev.* **2006**, *106*, 3561–3651. (c) Babu, S. A.; Krishnan, K. K.; Ujwaldev, S. M.; Anilkumar, G. Applications of Pybox Complexes in Asymmetric Catalysis. *Asian J. Org. Chem.* **2018**, *7*, 1033–1053.
- (14) See for example: (a) Hoyt, J. M.; Sylvester, K. T.; Semproni, S. P.; Chirik, P. J. Synthesis and Electronic Structure of Bis(imino)pyridine Iron Metallacyclic Intermediates in Iron-Catalyzed Cyclization Reactions. *J. Am. Chem. Soc.* **2013**, *135*, 4862–4887. (b) Appukuttan, V. K.; Liu, Y.; Son, B. C.; Ha, C.-S.; Suh, H.; Kim, I. Iron and Cobalt Complexes of 2,3,7,8-Tetrahydroacridine-4,5(1H,6)-diimine Sterically Modulated by Substituted Aryl Rind for the Selective Oligomerization to Polymerization of Ethylene. *Organometallics* **2011**, *30*, 2285–2294.
- (15) For computational studies on different PDI ligand modifications, see: (a) Zhu, D.; Budzelaar, P. H. M. Measure of σ -Donor and π -Acceptor Properties of Diiminepyridine-Type Ligands. *Organometallics* **2008**, *27*, 2699–2705. (b) Knijnenburg, Q.; Gambarotta, S.; Budzelaar, P. H. M. Ligand centred reactivity in diiminepyridine complexes. *Dalton. Trans.* **2006**, 5442–5448.
- (16) (a) Walker, I. C.; Palmer, M. H.; Hopkirk, A. The electronic states of the azines. II. Pyridine, studied by VUV absorption, near-threshold electron energy-loss spectroscopy and ab-initio multi-reference configuration interaction calculations. *Chem. Phys.* **1990**, *141*, 365–378. (b) Walker, I. C.; Palmer, M. H. The electronic states of the azines. IV. Pyrazine, studied by VUV absorption, near-threshold electron energy-loss spectroscopy and ab-initio multi-reference

configuration interaction calculations. *Chem. Phys.* **1991**, *153*, 169–187.

(17) Soscun Machado, H. J.; Hinchliffe, A. Relationship between the HOMO energies and the pK_a values in monocyclic and bicyclic azines. *J. Mol. Struct.: THEOCHEM* **1995**, *339*, 255–258.

(18) (a) Liberman-Martin, A. L.; Bergman, R. G.; Tilley, T. D. A Remote Lewis Acid Trigger Dramatically Accelerates Biaryl Reductive Elimination from a Platinum Complex. *J. Am. Chem. Soc.* **2013**, *135*, 9612–9615. (b) Liberman-Martin, A. L.; Levine, D. S.; Liu, W.; Bergman, R. G.; Tilley, T. D. Biaryl Reductive Elimination Is Dramatically Accelerated by Remote Lewis Acid Biding to a 2,2'-Bipyrimidyl-Platinum Complex: Evidence for a Bidentate Ligand Dissociation Mechanism. *Organometallics* **2016**, *35*, 1064–1069. (c) Goudy, V.; Jaoul, A.; Cordier, M.; Clavaguera, C.; Nocton, G. Tuning the Stability of Pd(IV) Intermediates Using a Redox Non-innocent Ligand Combined with an Organolanthanide Fragment. *J. Am. Chem. Soc.* **2017**, *139*, 10633–10636.

(19) For other routes to pyridine-based PDI ligands, see: (a) Gygi, D.; Hwang, S. J.; Nocera, D. G. Scalable Syntheses of 4-Substituted Pyridine-Diimines. *J. Org. Chem.* **2017**, *82*, 12933–12938. (b) Darnon, J. M.; Turner, Z. R.; Lobkovsky, E.; Chirik, P. J. Electronic Effects in 4-Substituted Bis(imino)pyridines and the Corresponding Reduced Iron Compounds. *Organometallics* **2012**, *31*, 2275–2285.

(20) (a) Beaufort, L.; Benvenuti, F.; Noels, A. F. Iron(II)-ethylene polymerization catalysts bearing 2,6-bis(imino)pyrazine ligands: Part I. Synthesis and characterization. *J. Mol. Catal. A: Chem.* **2006**, *260*, 210–214. (b) Beaufort, L.; Benvenuti, F.; Noels, A. F. Iron(II)-ethylene polymerization catalysts bearing 2,6-bis(imino)pyrazine ligands: Part II. Catalytic behaviour, homogenous and heterogenous insights. *J. Mol. Catal. A: Chem.* **2006**, *260*, 215–220. (c) Kolb, P.; Demuth, D.; Newsam, J. M.; Smith, M. A.; Sundermann, A.; Schunk, S. A.; Bettonville, S.; Breulet, J.; Francois, P. Parallel Synthesis and Testing of Catalysts for the Polymerization of Ethylene. *Macromol. Rapid Commun.* **2004**, *25*, 280–285.

(21) The ^1H and ^{13}C NMR spectra of the 2,6-diacetylpyrazine **3** and isomeric 2,5-diacetylpyrazine **6**, as well as their condensation follow-up products **4** and **7**, respectively, do not show any diagnostic signals which would allow one to differentiate them (see the [Supporting Information](#)). The preference for the 2,5-isomer can be rationalized through the fact that the α -carbon atom with respect to the protonated nitrogen in the Minisci coupling mechanism is more electron deficient and susceptible to radical attack. See: Fontana, F.; Minisci, F.; Nogueira Barbosa, M. C.; Vismara, E. Homolytic acylation of protonated pyridines and pyrazines with α -keto acids: the problem of monoacylation. *J. Org. Chem.* **1991**, *56*, 2866–2869.

(22) Although the iron center is formally electronically unsaturated ($16e^-$), the structure is monomeric in the crystalline state and resembles Milstein's pyrazine-based (PNP)FeBr₂ complex. While they are monomeric in solution, other pyrazine-based (PNP)Fe complexes undergo oligomerization in the solid state. See: Rivada-Wheelaghan, O.; Dauth, A.; Leitus, G.; Diskin-Posner, Y.; Milstein, D. Synthesis and Reactivity of Iron Complexes with a New Pyrazine-Based Pincer Ligand, and Application in Catalytic Low-Pressure Hydrogenation of Carbon Dioxide. *Inorg. Chem.* **2015**, *54*, 4526–4538.

(23) Addison, A. W.; Rao, T. N.; Reedijk, J.; van Rijn, J.; Verschoor, G. C. Synthesis, structure, and spectroscopic properties of copper(II) compounds containing nitrogen-sulphur donor ligands; the crystal and molecular structure of aqua[1,7-bis(*N*-methylbenzimidazol-2'-yl)-2,6-dithiaheptane]copper(II) perchlorate. *J. Chem. Soc., Dalton Trans.* **1984**, 1349–1356.

(24) The reported values of ν_{CO} for $(^{\text{IPr}}\text{PDI})\text{Fe}(\text{CO})_2$ of 1974 and 1914 cm^{-1} are in pentane solution.^{10a,b} As there can be up to a 20 cm^{-1} difference between ν_{CO} recorded in solution and in the solid state (see ref 22 for similar cases), the reported values in the main text are from our in-house ATR solid-state measurement of the reported complex. For compounds **9**, [**10**]**I**, and **11** we have also recorded the IR spectra in solution, all of which show 11–25 cm^{-1} deviations to higher frequencies in comparison to solid-state data (see [Table 1](#)).

(25) Tondreau, A. M.; Milsmann, C.; Lobkovsky, E.; Chirik, P. J. Oxidation and Reduction of Bis(imino)pyridine Iron Dicarboxyl Complexes. *Inorg. Chem.* **2011**, *50*, 9888–9895.

(26) For PDI systems, see ref 10. For PNN systems, see: (a) Butschke, B.; Fillman, K. L.; Bendikov, T.; Shimon, L. J. W.; Diskin-Posner, Y.; Leitus, G.; Gorelsky, S. I.; Neidig, M. L.; Milstein, D. How Innocent are Potentially Redox Non-Innocent Ligands? Electronic Structure and Metal Oxidation States in Iron-PNN Complexes as a Representative Case Study. *Inorg. Chem.* **2015**, *54*, 4909–4926. (b) Zell, T.; Milko, P.; Fillman, K. L.; Diskin-Posner, Y.; Bendikov, T.; Iron, M. A.; Leitus, G.; Ben-David, Y.; Neidig, M. L.; Milstein, D. Iron Dicarboxyl Complexes Featuring Bipyridine-Based PNN Pincer Ligands with Short Interpyridine C—C Bond Lengths: Innocent or Non-Innocent Ligand? *Chem. - Eur. J.* **2014**, *20*, 4403–4413.

(27) $\Delta = 0.0772$ was obtained using the metric data from both entities of **9** present in the asymmetric unit and is nearly identical with the single structural parameter we calculated for $(^{\text{IPr}}\text{PDI})\text{Fe}(\text{CO})_2$ ($\Delta = 0.071$) reported by Chirik.²⁵ See: Römel, C.; Weyhermüller, T.; Wieghardt, K. Structural characteristics of redox-active pyridine-1,6-diimine complexes: Electronic structures and ligand oxidation levels. *Coord. Chem. Rev.* **2019**, *380*, 287–317.

(28) All calculations were performed with ORCA 4.1.2: (a) Neese, F. The ORCA program system. *Wiley Interdiscip. Rev.: Comput. Mol. Sci.* **2012**, *2*, 73–78. (b) Neese, F. Software update: the ORCA program system, version 4.0. *Wiley Interdiscip. Rev.: Comput. Mol. Sci.* **2018**, *8*, No. e1327.

(29) For details on the calculation of Mössbauer parameters see the [Supporting Information](#). The calibration was performed using the linear regression from: Pápai, M.; Vankó, G. On Predicting Mössbauer Parameters of Iron-Containing Molecules with Density-Functional Theory. *J. Chem. Theory Comput.* **2013**, *9*, 5004–5020.

(30) For explanations regarding the BS(m,n) notation, see the Computational Section of the [Supporting Information](#).

(31) Neese, F. Definition of corresponding orbitals and diradical character in broken symmetry DFT calculations on spin coupled systems. *J. Phys. Chem. Solids* **2004**, *65*, 781–785.

(32) Tang, S.; von Wolff, N.; Diskin-Posner, Y.; Leitus, G.; Ben-David, Y.; Milstein, D. Pyridine-Based PCP-Ruthenium Complexes: Unusual Structures and Metal-Ligand Cooperation. *J. Am. Chem. Soc.* **2019**, *141*, 7554–7561.

(33) The stronger back-bonding-stabilized interactions between metal centers and pyrazinium salts has been both experimentally and computationally documented in the systems of the type $[\text{Fe}(\text{CN})_5(\text{Mepyrazinium})]^+$. See for example: (a) Formiga, A. L. B.; Vancoillie, S.; Pierloot, K. Electronic Spectra of N-Heterocyclic Pentacyanoferrate(II) Complexes in Different Solvents, Studied by Multiconfigurational Perturbation Theory. *Inorg. Chem.* **2013**, *52*, 10653–10663. (b) Estrin, D. A.; Hamra, O. Y.; Paglieri, L.; Slep, L. D.; Olabe, J. A. Structure and Bonding in Pentacyano(L)ruthenate(II) Complexes (L = Pyridine, Pyrazine, and N-Methylpyrazinium): A Density Functional Study. *Inorg. Chem.* **1996**, *35*, 6832–6837.

(34) For related examples where metal-ligated fragments undergo reductive, albeit irreversible, dimerization, see: (a) Lapointe, S.; Khaskin, E.; Fayzullin, R. R.; Khusnutdinova, J. R. Nickel(II) Complexes with Electron-Rich, Sterically Hindered PNP Pincer Ligands Enable Uncommon Modes of Ligand Dearomatization. *Organometallics* **2019**, *38*, 4433–4447. (b) Watanabe, M.; Sato, M.; Takayama, T. A Novel Coordination Mode of the Fulvalene Ligand in Binuclear Ruthenium Complexes. Synthesis, Structure, and Some Reactivities of $[(\eta^5\text{-Cp})\text{Ru}(\mu_2\text{-}\eta^6\text{-}\eta^6\text{-C}_{10}\text{H}_8)\text{Ru}(\eta^5\text{-Cp})](\text{BF}_4)_2$. *Organometallics* **1999**, *18*, 5201–5203. (c) Mohapatra, S. K.; Fonari, A.; Risko, C.; Yesudas, K.; Mpugil, K.; Delcamp, J. H.; Timofeeva, T. V.; Bredas, J.-L.; Marder, S. R.; Barlow, S. Dimers of Nineteen-Electron Sandwich Compounds: Crystal and Electronic Structures, and Comparison of Reducing Strengths. *Chem. - Eur. J.* **2014**, *20*, 15385–15394. (d) Daw, P.; Kumar, A.; Oren, D.; Espinosa-Jalapa, N. A.; Srimani, D.; Diskin-Posner, Y.; Leitus, G.; Shimon, L. J. W.; Carmieli, R.; Ben-David, Y.; Milstein, D. Redox Noninnocent Nature

of Acridine-Based Pincer Complexes of 3d Metals and C–C Bond Formation *Organometallics*, **2020**, DOI: 10.1021/acs.organomet.9b00607.

(35) The standard C(sp³)–C(sp³) bond distance is 1.54 Å: *CRC Handbook of Chemistry and Physics*, 93rd ed.; Haynes, W., Ed.; CRC Press: Boca Raton, FL, 2012.

(36) We note that in certain organic radical dimers, C(sp³)–C(sp³) bond lengths to up to 1.71 Å have been observed. See for example: Schreiner, P. R.; Chernish, L. V.; Gunchenko, P. A.; Tikhonchuk, E. Y.; Hausmann, H.; Serafin, M.; Schlecht, S.; Dahl, J. E. P.; Carlson, R. M.; Fokin, A. A. Overcoming lability of extremely long carbon-carbon bonds through dispersion forces. *Nature* **2011**, *477*, 308–311 and references therein.

(37) For another example where a diradical could be cleaved oxidatively, see: (a) Hsu, S. C. N.; Yeh, W.-Y.; Lee, G.-H.; Peng, S.-M. Reductive Dimerization and Thermal Rearrangement of Biphenylene Coordinated to Tricarbonylmanganese. *J. Am. Chem. Soc.* **1998**, *120*, 13250–13251. For examples where ligand-centered radicals are in equilibrium with their dimeric analogues, see: (b) Nocton, G.; Lukens, W. W.; Booth, C. H.; Rozenel, S. S.; Medling, S. A.; Maron, L.; Andersen, R. A. Reversible Sigma C–C Bond Formation Between Phenanthroline Ligands Activated by (C₅Me₅)₂Yb. *J. Am. Chem. Soc.* **2014**, *136*, 8626–8641. (c) Liu, B.; Yoshida, T.; Li, X.; Stepien, M.; Shinokubo, H.; Chmielewski, P. J. Reversible Carbon-Carbon Bond Breaking and Spin Equilibria in Bis(pyrimineno)corrole. *Angew. Chem., Int. Ed.* **2016**, *55*, 13142–13146. (d) Andrez, J.; Guidal, V.; Scopelliti, R.; Pecaut, J.; Gambarelli, S.; Mazzanti, M. Ligand and Metal Based Multielectron Redox Chemistry of Cobalt Supported by Tetradentate Schiff Bases. *J. Am. Chem. Soc.* **2017**, *139*, 8628–8638.